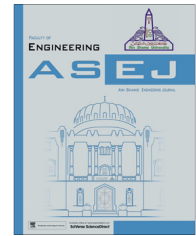




Ain Shams University

Ain Shams Engineering Journal

www.elsevier.com/locate/asej  
www.sciencedirect.com



ELECTRICAL ENGINEERING

# Decoupled control of grid connected photovoltaic system using fractional order controller

M. Lakshmi \*, S. Hemamalini

School of Electrical Engineering, VIT University, Chennai, India

Received 4 January 2016; accepted 2 June 2016

## KEYWORDS

PV array;  
High gain multilevel DC/DC  
converter;  
MPPT control;  
Decoupled control;  
THD;  
PI and FO-PI controller

**Abstract** In a grid connected photovoltaic (PV) system, dynamic control strategy is essential to use the solar energy efficiently as well as for an energy optimization. This paper presents a decoupled control of grid connected photovoltaic system using Fractional Order Proportional–Integral (FO-PI) controller. In the proposed system, closed loop high gain multilevel DC/DC converter is also implemented to meet the regulated DC link voltage at the inverter input. The decoupled control strategy allows independent control of real power ( $P$ ) and reactive power ( $Q$ ) according to the power generated by photovoltaic systems and the power consumed by the utility grid. A complete study of the dynamic behavior of the grid connected PV system is presented using Matlab/Simulink. Simulation results are presented to validate the system response during disturbance with FO-PI controller, power factor control at the grid and the Total Harmonic Distortion (THD) of grid current for any solar irradiation.

© 2016 Faculty of Engineering, Ain Shams University. Production and hosting by Elsevier B.V. This is an open access article under the CC BY-NC-ND license (<http://creativecommons.org/licenses/by-nc-nd/4.0/>).

## 1. Introduction

With the increasing concern about global warming, the necessity to generate pollution-free power is the need of the hour. The photovoltaic (PV) generation system is one of the best renewable energy sources available to meet out the energy crisis. It is safe, clean, pollution-free, and it requires less maintenance and inexhaustible. The standalone PV system is widely used in remote areas where the power generation is needed.

The use of energy storage devices in the standalone system increases the overall cost of the system. Hence, the three-phase grid connected system is considered to reduce the investment cost. The PV array is connected to utility grid through converters and inverters. Due to the presence of power electronic devices, it is necessary to maintain THD standards, grid current control during normal/faulty conditions and grid synchronization [1,2].

In general, the voltage obtained from the PV array is very low and has to be boosted considerably for the grid applications. The conventional boost converters are not suitable for higher power applications due to extreme increases in duty cycle to achieve higher voltage gain. In most of the grid connected system, interleaved and cascaded boost converters are used widely used to achieve the required high voltage gain [3–6]. However, cascading of boost converters has drawbacks of incremental costs and complexity of the control circuit even

\* Corresponding author. Mobile: +91 9003037797.

E-mail address: [lakshmi.m@vit.ac.in](mailto:lakshmi.m@vit.ac.in) (M. Lakshmi).

Peer review under responsibility of Ain Shams University.



Production and hosting by Elsevier

<http://dx.doi.org/10.1016/j.asej.2016.06.002>

2090-4479 © 2016 Faculty of Engineering, Ain Shams University. Production and hosting by Elsevier B.V.

This is an open access article under the CC BY-NC-ND license (<http://creativecommons.org/licenses/by-nc-nd/4.0/>).

Please cite this article in press as: Lakshmi M, Hemamalini S, Decoupled control of grid connected photovoltaic system using fractional order controller, Ain Shams Eng J (2016), <http://dx.doi.org/10.1016/j.asej.2016.06.002>

it achieves high voltage gain. In addition, efficiency and gain of the system is restricted due to high ripple current and higher losses. Interleaved converter uses transformers or coupled inductor to achieve required high gain with necessary turns ratio [7–10]. The increase in turns ratio results in high leakage in the secondary that causes increased switching loss at the output. Further, these topologies have the drawbacks of limited switching frequency, high voltage stress and transformer losses. From the literature, gain and efficiency of the converter in the grid connected PV system is increased by implementing the transformer less topology. To overcome these issues, a high gain multilevel DC/DC converter is used to achieve the required high gain in the grid-connected applications [11–13]. The lower rating devices are used in multilevel converter owing to fixed and equal voltage stress on each stage of the device that is lower than the output voltage. The low on-state resistance of the switch reduces the conduction losses and improves efficiency.

For many years, Proportional–Integral (PI) controllers are popular in grid connected PV applications, to control the system parameters under disturbances. The main features of PI controller are simple design procedure and good performance characteristics. Owing to the wide usage of PI controllers, it is necessary to improve their quality and robustness [14,15]. The performance of PI controller is enhanced by introducing FO-PI controller whose integral order is non-integer. The increase in tuning parameters of FO-PI controller, increases the robustness of the system, provides optimal control and delivers better system response than the PI controller [16].

In this paper, a decoupled control strategy for grid-connected PV system with high gain DC/DC converter and FO-PI controller is presented for power quality studies. A high gain multilevel DC/DC converter is employed for the proposed 1KW grid-connected PV system to generate the required DC link voltage at the inverter input. This grid-connected system comprises of the required control features that provide regulation of inverter current through FO-PI controller to meet the power quality standards of the grid. In addition, it gives significant reduction in the grid current THD. This control strategy enables power factor control, reactive power compensation

and synchronization through PLL, in order to achieve grid code agreement during voltage unbalances.

## 2. Modeling of three phase grid-connected photovoltaic system

A three phase grid-connected PV system is illustrated in Fig. 1 with two-stage of control operation. The first stage uses a high gain multilevel DC/DC converter, which is employed to maintain the DC link voltage as constant. In addition, this converter makes the PV array to operate at the optimal operating point with the use of MPPT control during the variation in environmental conditions. In the second stage, a DC–AC inverter is used to convert the DC power into an AC power and controls the output current. The purpose of the decoupled control of the grid connected photovoltaic inverter is to transfer the maximum power supplied from PV panel to the utility as efficiently as possible [17,18]. The control requirement of the system is supported with the SPWM control techniques.

### 2.1. PV Array modeling

Fig. 2 shows the equivalent circuit model of a PV cell. Series-parallel combination of PV cells forms a PV panel with specified rating of voltage and current. The output current and voltage of a PV cell is expressed in Eq. (1)

$$I = I_{ph} - I_{rs} \left[ e^{\left( \frac{q}{kT} \frac{V}{n_s} \right)} - 1 \right] \quad (1)$$

where  $V$  is the cell voltage,  $K$  is the Boltzmann constant,  $q$  is the charge of an electron and  $A$  is the diode ideality factor.  $T$  is the absolute temperature [19]. The photocurrent ( $I_{ph}$ ) and the reverse saturation current ( $I_{rs}$ ) of the PV cell is given in Eqs. (2) and (3).

$$I_{ph} = [I_{scr} + \lambda(T - T_r)] \frac{S}{1000} \quad (2)$$

$$I_{rs} = I_{rr} * \left[ \frac{T}{T_r} \right]^3 * \left[ e^{\left( \frac{qE_{Gs}}{kT} \left[ \frac{1}{T_r} - \frac{1}{T} \right] \right)} - 1 \right] \quad (3)$$

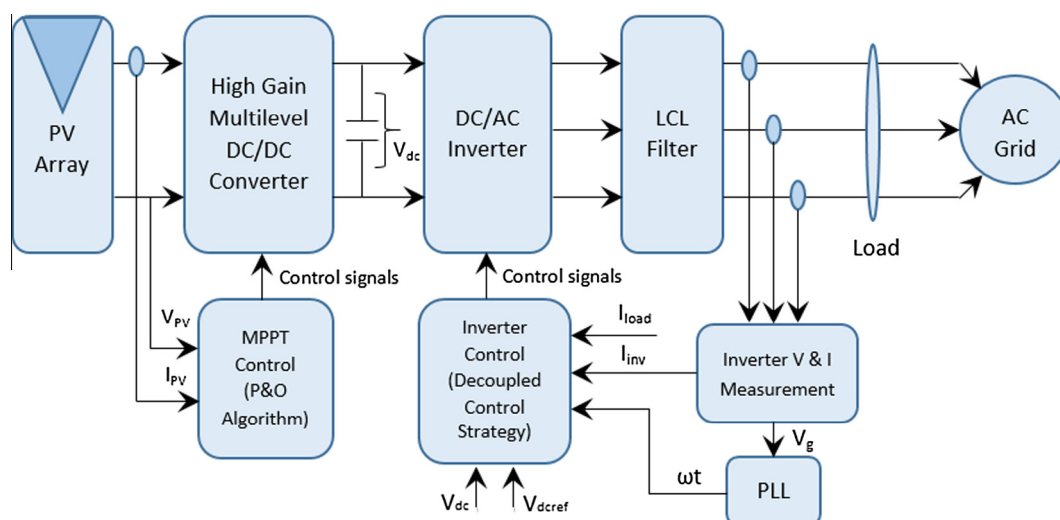


Figure 1 Three phase grid-connected PV system.

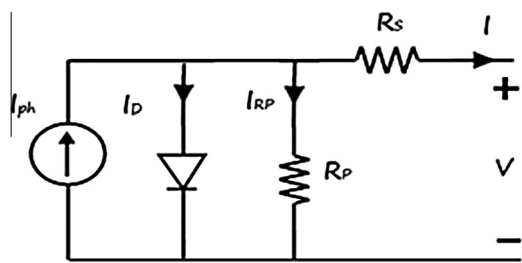


Figure 2 Equivalent circuit model of solar cell.

where  $I_{sc}$  is the short circuit current at the reference temperature,  $S$  is the solar irradiation,  $\lambda$  is the temperature coefficient,  $T_r$  is the reference temperature,  $I_{rr}$  is the reverse saturation current at reference temperature and  $E_G$  is the energy band-gap.

Eq. (4) gives the output current for a PV module/array

$$I = n_p I_{ph} - n_p I_{rs} \left[ e^{\left( \frac{q}{kT_r} \frac{V}{n_s} \right)} - 1 \right] \quad (4)$$

where  $n_s$  and  $n_p$  are the number of series and parallel cells.

The selection of PV cells are mainly based on open circuit voltage ( $V_{oc}$ ), short circuit current ( $I_{sc}$ ), optimal operating point, fill factor and efficiency of solar cell [20]. The open circuit voltage and short circuit current are directly proportional to the temperature and the photocurrent respectively. The amount of power generated by the PV panel is based on the available solar irradiation, temperature and the size of the panel. The PV array size depends on the power requirement of the grid. The parameters and description of four 250 W solar PV panel selected for 1 kW PV array are shown in Table 1.

### 2.2. High gain multilevel DC/DC converter

Fig. 3 shows the high gain multilevel DC/DC converter topology. It consists of conventional boost converter with additional capacitors and diodes to increase the gain of the converter. This converter has one switch, 2 N-1 diodes and capacitors. The output voltage  $V_o$  is  $N * V_c$ , where  $V_c$  is the capacitor voltage and  $N$  is the number of levels in the converter [21].

The voltage gain for the high gain multilevel DC/DC converter can be obtained using (5).

$$\text{Voltage gain} = \frac{N}{1 - D} \quad (5)$$

where  $D$  is the duty ratio. The value of inductance ( $L$ ) and capacitance ( $C$ ) are determined using (6) and (7), which is similar to the conventional boost converter [22].

$$L = \frac{D(1 - D)^2 R}{2f} \quad (6)$$

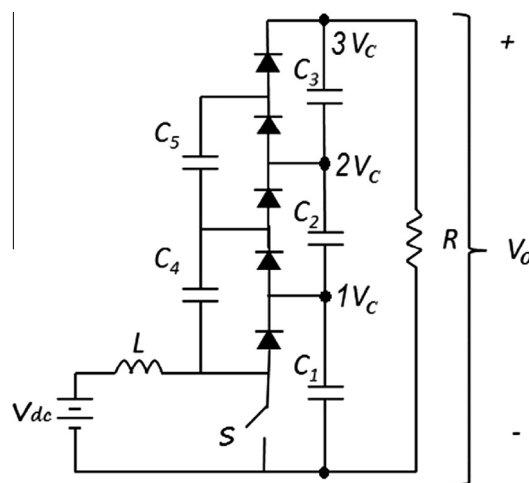


Figure 3 High gain multilevel DC/DC converter.

$$C = \frac{DV_o}{fV_r R} \quad (7)$$

where  $f$  is the switching frequency,  $R$  is the load resistor,  $V_r$  is voltage ripple factor and  $V_o$  is the output voltage.

### 2.3. MPPT control

P&O algorithm is widely used to operate the PV panel at the optimized operating point due to its simple structure. This MPPT algorithm operates periodically by comparing the PV output power with that of the previous perturbation cycle. Based on the change in power ( $\Delta P$ ), the PV array voltage is incremented or decremented to reach MPP. This algorithm is summarized in Table 2. P&O algorithm obeys for the instantaneous value of PV array voltage and current, if sampling occurs only once in each switching cycle. The MPPT process is recurring periodically until the optimal operating point is reached. The system then oscillates near the MPP. The oscillation is minimized by reducing the perturbation step size. However, a smaller perturbation size slows down the MPPT [23]. Fig. 4 shows the flow chart of conventional P&O technique.

### 2.4. Control of DC/AC inverter

In a grid-connected PV system, inverter control comprises of two control loops. The inner control loop is employed to regulate the DC-link voltage of the system for balancing the power flow and maintains the stability during dynamics. In addition, the outer control loop with a SPWM technique is used to control the current which is injected into the grid at unity power factor with low harmonic distortions

Table 1 Parameters of PV panel SPSM250 at STC.

Parameters	Values (unit)
Peak power ( $P_{max}$ )	250W <sub>p</sub>
Open circuit voltage ( $V_{oc}$ )	43.21 V
Short circuit current ( $I_{sc}$ )	7.63 A
Voltage at max power ( $V_{mp}$ )	35.5 V
Current at max power ( $I_{mp}$ )	7.04 A
No. of cells ( $n_s$ )	72

Table 2 Summary of P&O algorithm.

Perturbation	Change in power ( $\Delta P$ )	Next perturbation
Positive	Positive	Positive
Positive	Negative	Negative
Negative	Positive	Negative
Negative	Negative	Positive

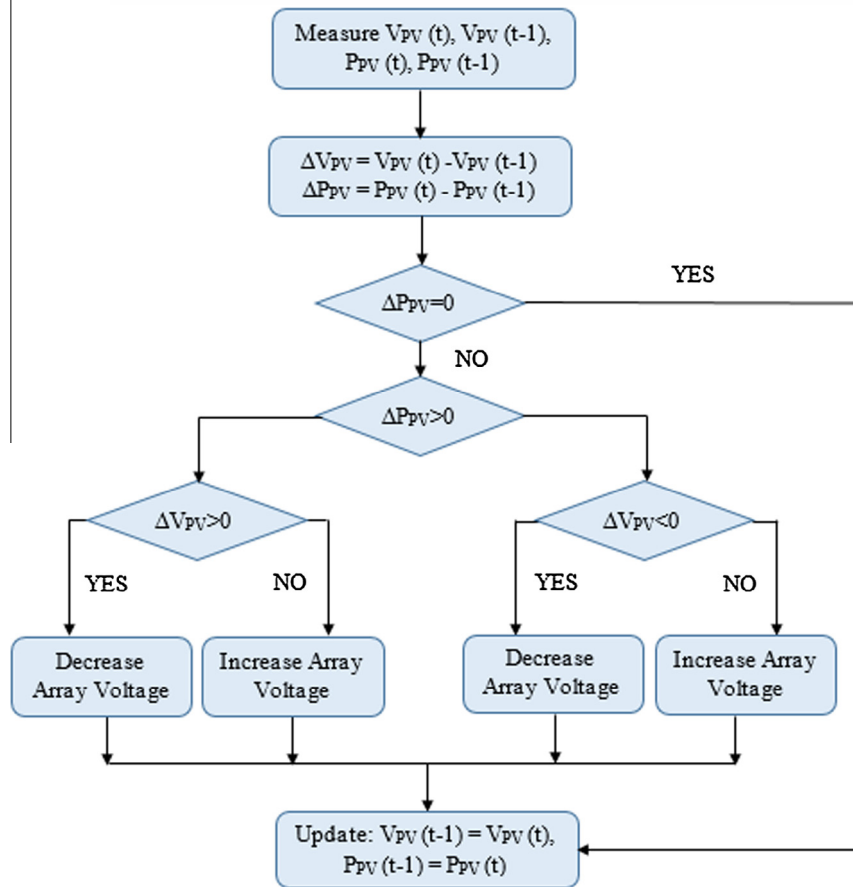


Figure 4 Flow chart for P&O algorithm.

(THD < 5%). The decoupled current control strategy is responsible for power quality issues and current harmonic compensation. As well, a Phase Locked Loop (PLL) device is used to generate a synchronized reference current to the current control loop.

Decoupled control of inverter with FO-PI controller performs two independent control of active and reactive power between the PV system and the grid. From the inverter, the quality real power is fed into the grid at unity power factor. Together, the reactive power compensation is carried out based on the utility demand and the PV generated power [24]. Though the real power ( $P$ ) and reactive power ( $Q$ ) of the inverter are determined from the apparent power ( $S$ ) such that [25]:

$$S = P + jQ \quad (8)$$

where

$$P = \frac{V_g}{\omega L} V_{inv} \sin \delta \quad (9)$$

$$Q = \frac{V_g}{\omega L} (V_g - V_{inv} \cos \delta) \quad (10)$$

The phase angle between the grid voltage  $V_g$  and the inverter output voltage  $V_{inv}$  is denoted as  $\delta$ . The real and reactive power exchanged with the utility grid is determined from Eqs. (9) and (10) and is dependent on the phase angle ( $\delta$ ) and the inverter output voltage magnitude ( $V_{inv}$ ). The  $d-q$  cur-

rent components are settled with suitable values during the entire operating time to control both real and reactive power. During nighttime, the PV generator is failed to supply real power. Hence, the inverter carries out the reactive power compensation. The real power supplied by the inverter increases during daytime and satisfies the needs of utility grid, thereby reduces the reactive power flow.

From Fig. 5, the inverter active current component ( $i_{dinv}$ ) and the inner DC voltage controller determines the reference active component ( $i_{dref}$ ). The reference reactive component ( $i_{qref}$ ) is obtained by the reactive current component of the inverter ( $i_{qinv}$ ) and the load ( $i_{qload}$ ). From Eqs. (11) and (12), the reference active and reactive component is maintained at specified value with the use of FO-PI controller during the variations of environment conditions.

$$i_{dref} = \left[ \left( K_{Pdc} + \frac{K_{Idc}}{S^{i_{dc}}} \right) (V_{dc} - V_{dcref}) - i_{dinv} \right] \left( K_P + \frac{K_I}{S^i} \right) \quad (11)$$

$$i_{qref} = [i_{qload} - i_{qinv}] \left( K_P + \frac{K_I}{S^i} \right) \quad (12)$$

## 2.5. FO-PI controllers

The block diagram of FO-PI controller is shown in Fig. 6. This controller is denoted as  $PI^i$ . The FO-PI controller is an extension of classical PI controller. [11,12].

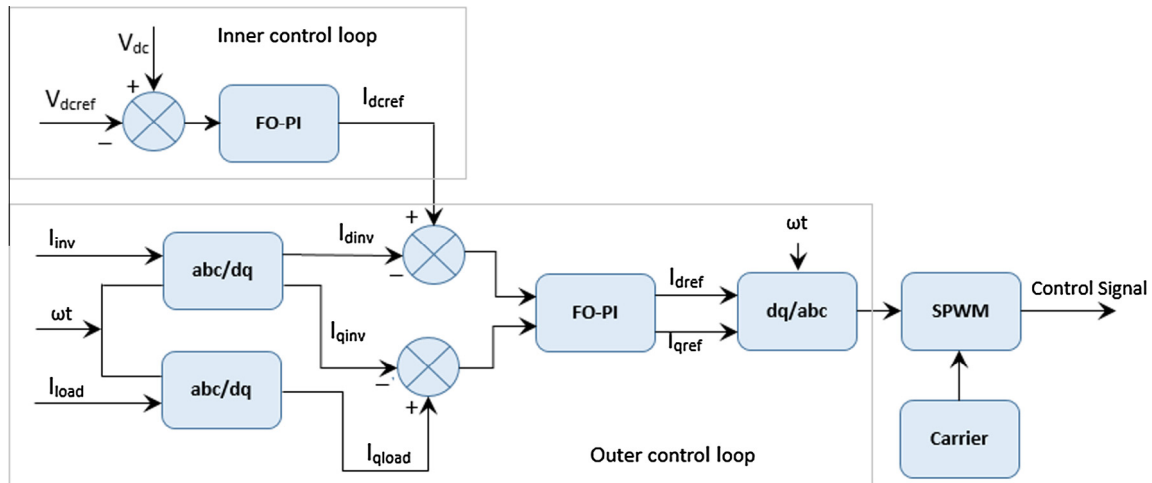


Figure 5 Decoupled control strategy.

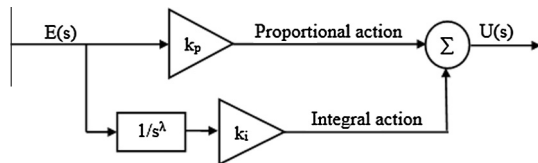


Figure 6 Block diagram of FO-PI controller.

The differential equation of fractional order controller is,

$$u(t) = (k_p + k_i D_t^{-\lambda})e(t) \quad (13)$$

where  $e(t)$  is the error signal and  $u(t)$  is the control signal.

The continuous transfer function of the FO-PI controller is given by

$$\frac{U(S)}{E(S)} = k_p + k_i S^{-\lambda} \quad (14)$$

where  $\lambda$  is an arbitrary real number. A classical PI controller is achieved by assuming  $\lambda = 1$ . Thus, the modification in PI controller provides flexibility and accuracy in the FO-PI controller. The increase in robustness makes the system more stable. The optimal values of FOPID controller parameters are tuned with Ziegler Nicholas method to control the overall system performance.

In this system, two control loops are considered: an inner control loop, and an outer control loop. The FO-PI controller is used to control the DC voltage at the inner control loop by comparing the DC link voltage with the reference DC voltage. This control loop keeps the DC link voltage as constant and efficiently transfers power from the PV system to the grid. In the outer control loop, the real and reactive components are controlled by the FO-PI controller and allowing the synchronization between the inverter and the grid voltages.

### 2.6. LCL filter

According to IEEE 519 standard, the THD of the three phase currents lie around 5% [26]. In addition, the power delivered to the grid must assure the power quality requirements. The LCL filter is presented to meet the standard for interconnecting the PV-grid system. The inductance of a LCL filter is small as compared to the  $L$  filter to minimize the harmonics at the

switching frequency. The increase in amplitude at resonant frequency causes instability of the overall system. To overcome this disadvantage, a damping resistor  $R$  is introduced [27]. Fig. 7 shows the equivalent circuit of an LCL filter and the parameters are calculated by the following equations. The inverter side inductance ( $L_{inv}$ ) is expressed in Eq. (15) w.r.t dc link voltage ( $V_{dc}$ ), rated ripple current ( $\Delta I_{Lmax}$ ) and the switching frequency ( $f_s$ ) of the system.

$$L_{inv} = \frac{V_{dc}}{16 \cdot \Delta I_{Lmax} \cdot f_s} \quad (15)$$

In Eq. (16), a 10% ripple of rated current for 50% duty cycle is calculated from the nominal power ( $P_n$ ) and the phase voltage ( $V_{ph}$ ).

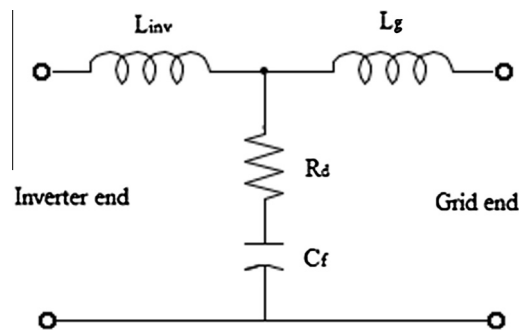


Figure 7 Equivalent circuit of LCL filter.

Table 3 Specifications for the grid-connected PV system.

Parameters	Values (unit)
PV array	1 kW
Grid voltage	3 $\phi$ , 440 V
Grid frequency	50 Hz
Switching frequency	5 kHz
DC link voltage	740 V
DC link capacitor	470 $\mu$ F
Output filter	$L_i = 20$ mH $L_g = 10$ mH $C_f = 1$ $\mu$ F

$$\Delta I_{Lmax} = 0.1 * \frac{P_n \sqrt{2}}{3 \cdot V_{ph}} \quad (16)$$

$$L_g = r * L_{inv} \quad (17)$$

The grid side inductance ( $L_g$ ) is expressed in Eq. (17) and it is calculated w.r.t. the relation factor ( $r$ ).

From Eq. (18), the filter capacitor ( $C_f$ ) is determined by multiplying the power factor variation at the grid with the base impedance of the system.

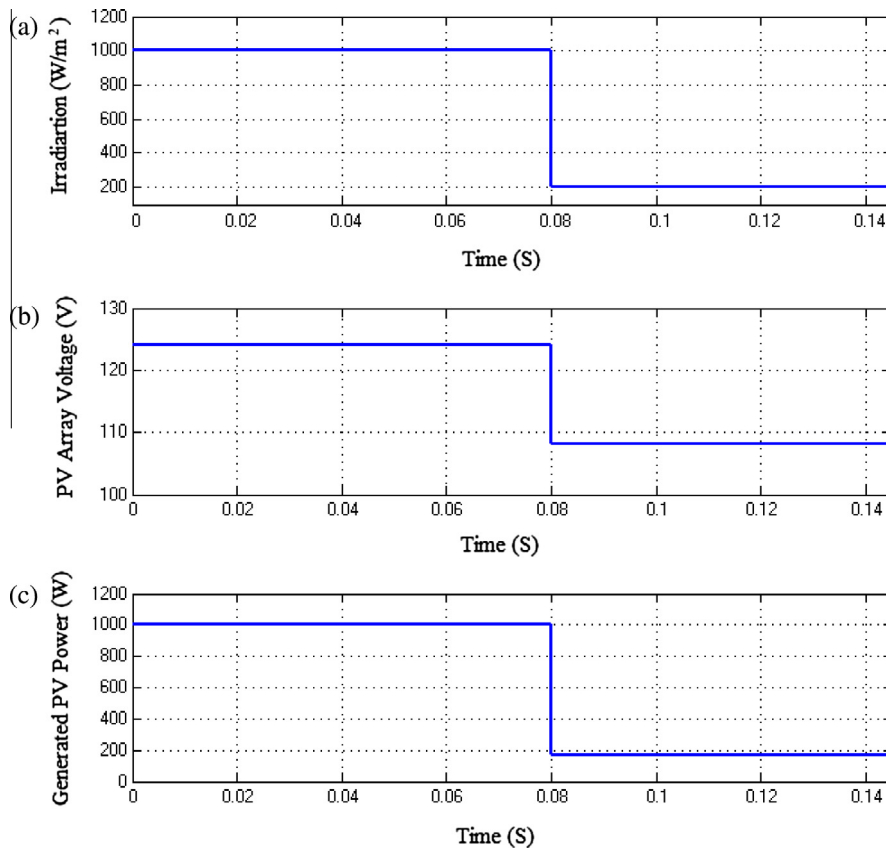


Figure 8 (a) Irradiation, (b) PV array voltage and (c) generated PV power.

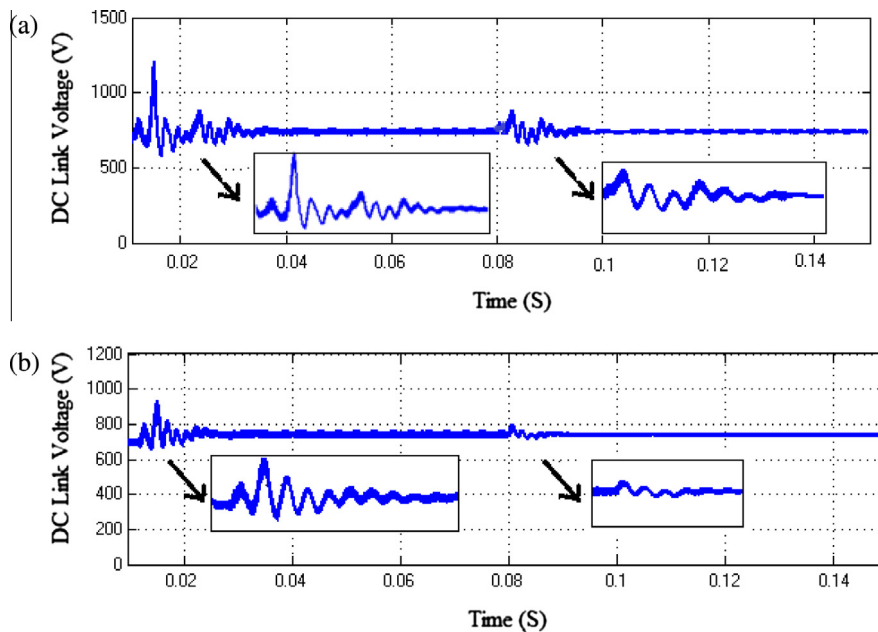
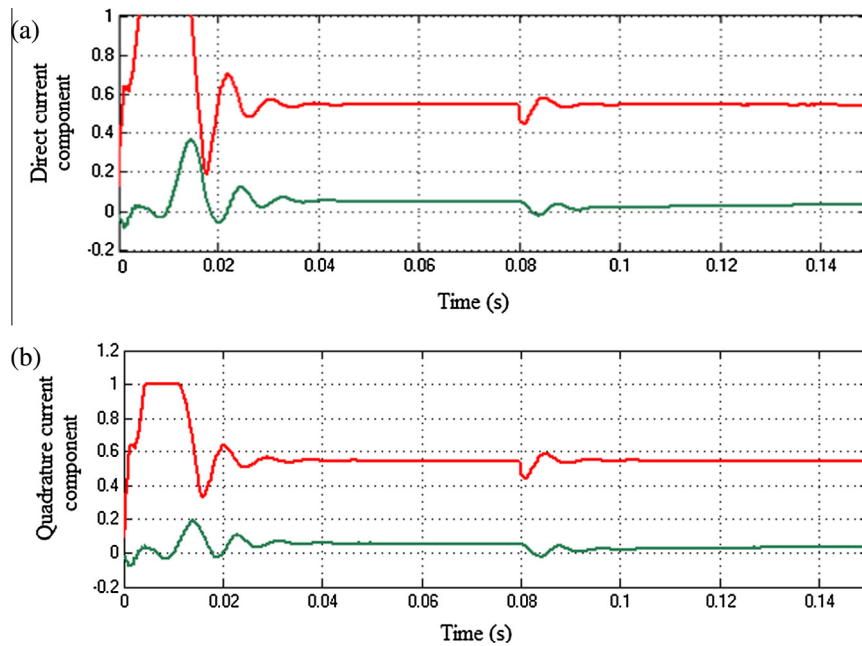
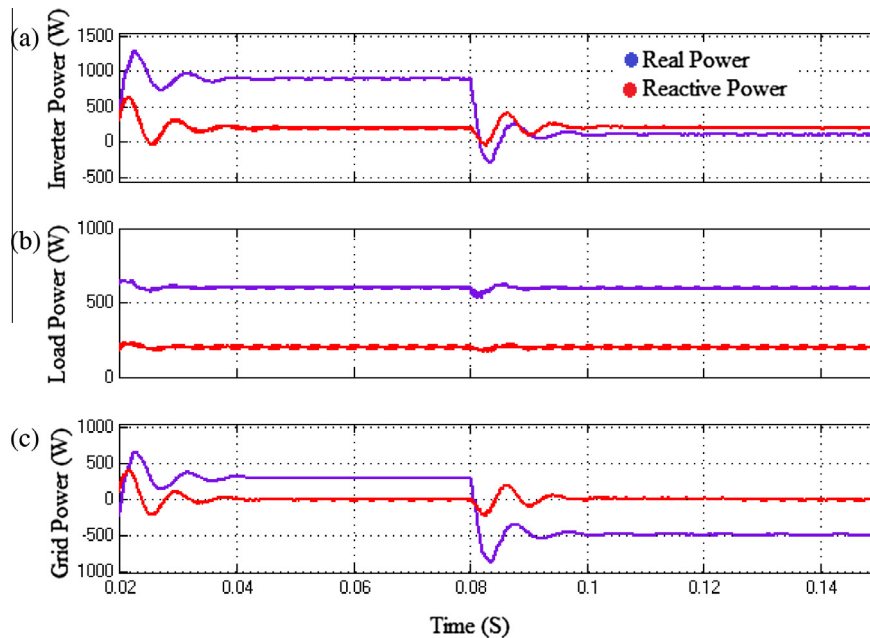


Figure 9 DC link voltage. (a) PI and (b) FO-PI controller.



**Figure 10** Direct and quadrature current component. (a) PI and (b) FO-PI controller.



**Figure 11** Real and reactive power during variable irradiation – FO-PI application. (a) Inverter, (b) load and (c) grid.

$$C_f = 0.05 * C_b \quad (18)$$

The damping resistor ( $R_d$ ) required to avoid resonance is obtained w.r.t resonant frequency ( $\omega_{res}$ ) and is given in Eqs. (19) and (20)

$$R_d = \frac{1}{3 \cdot C_f \cdot \omega_{res}} \quad (19)$$

$$\omega_{res} = \sqrt{\frac{L_{inv} + L_g}{L_{inv} \cdot L_g \cdot C_f}} \quad (20)$$

### 3. Simulation results and discussion

Fig. 1 shows the block diagram of decoupled control of grid-connected PV system. The overall system is simulated and analyzed in Matlab/Simulink platform. The parameters chosen to simulate the system are shown in Table 3. The behavior of three-phase grid connected PV system is investigated with PI and FO-PI controller for variable irradiation and load conditions.

**Table 4** Grid current THD during variable irradiation.

Irradiation (W/m <sup>2</sup> )	% THD	
	PI	FO-PI
1000	1.82%	1.24%
200	2.54%	1.87%

### 3.1. Controller performance under variable irradiation

In this case, initially the irradiation is set as 1000 W/m<sup>2</sup>. At  $t = 0.08$  s, the irradiation is changed to 200 W/m<sup>2</sup> as shown in Fig. 8(a). The generated PV array voltage corresponding to the variable irradiation is 124 V and 98 V respectively as shown in Fig. 8(b).

From the variable PV array voltage, aDCLink voltage of 740 V is obtained using high gain multilevel DC/DC converter. This DC link voltage is regulated by comparing the DC voltage reference with the output voltage of the converter and the error signal is given to the controller. Fig. 9(a) shows that the regulated DC link voltage ( $V_{dc}$ ) of 740 V, which settles at  $t = 0.036$  s and the peak overshoot voltage is 1240 V while implementing PI controller. The proportional ( $k_p$ ) and integral ( $k_i$ ) constant are obtained using Ziegler Nichols tuning as 0.0001 and 0.5 respectively.

Similarly, the settling time of direct ( $d$ ) and quadrature ( $q$ ) current component output in the outer control loop using PI controller is shown in Fig. 10(a). Whereas, the FO-PI controller makes the  $V_{dc}$  to settle at  $t = 0.024$  s and the peak over-

shoot is reduced to 926 V and is shown in Fig. 9(b). The controller parameters of FO-PI are same as PI controller constants.

In addition, fractional integral order ( $\lambda$ ) is introduced as 0.95 to improve the system performance. From the FO-PI controller output, reduction in settling period by 33% and peak overshoot voltage by 25.3% is achieved compared to PI controller. Likewise, the settling time of direct ( $d$ ) and quadrature ( $q$ ) current component output in the outer control loop using FO-PI is shown in Fig. 10(b). The control of  $dq$  current component allows the real and reactive power exchange between the inverter and the grid. The mathematical expression, which connects the real power supplied by the inverter, grid and the load, is given by

$$P_{Inv} = P_L \pm P_G \quad (21)$$

where  $P_{Inv}$  is the power delivered by the inverter,  $P_L$  is the power consumed by the load and  $P_G$  is the grid power. The real and reactive power delivered by the inverter during the irradiation of 1000 W/m<sup>2</sup> is 896 W and 200 VAR. The inverter power satisfies the load demand of 600 W, 200 VAR and the excess power is fed into the grid. During 200 W/m<sup>2</sup> irradiation, the power supplied by the inverter is 246 W, 200 VAR. Now, the required load demand is satisfied by delivering the real power of 354 W from the grid. Hence, Fig. 11 shows the real and reactive power exchange and the grid power factor is maintained unity by sustaining the reactive power is zero. From these results, the PV fed inverter acts as energy generator during daytime and acts as reactive power compensator during nighttime.

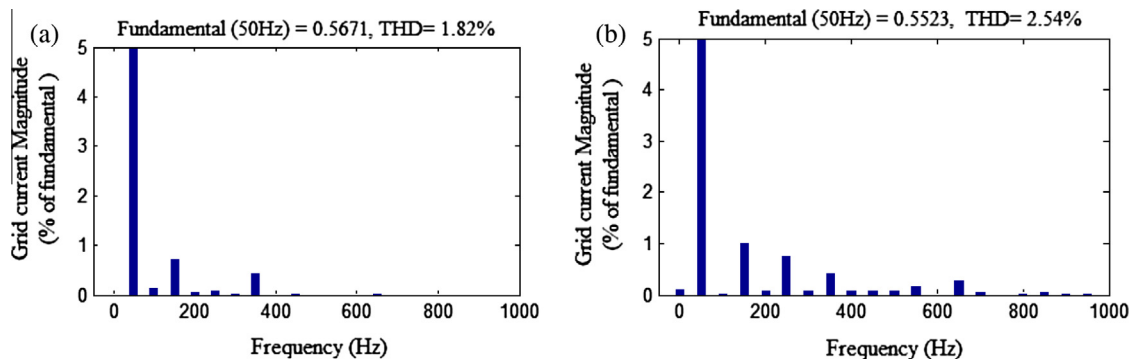


**Figure 12** FFT analysis of grid current THD under variable irradiation – PI application (a) for 1000 W/m<sup>2</sup> (b) for 200 W/m<sup>2</sup>.

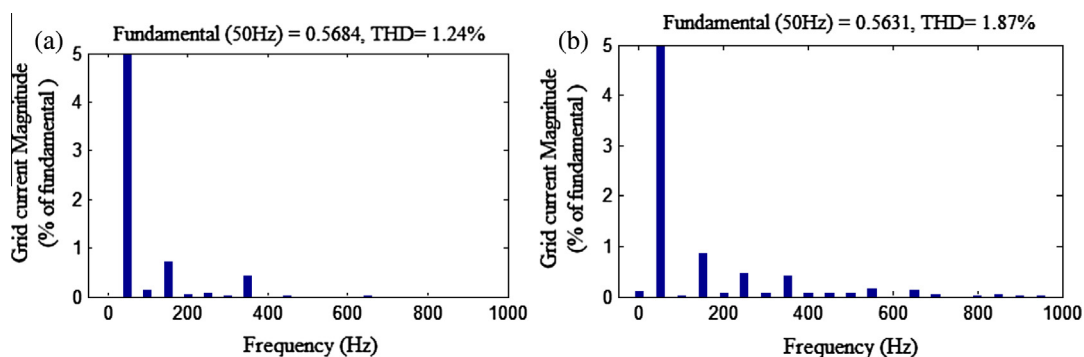


**Figure 13** FFT analysis of grid current THD under variable irradiation FO-PI application (a) for 1000 W/m<sup>2</sup> (b) for 200 W/m<sup>2</sup>.

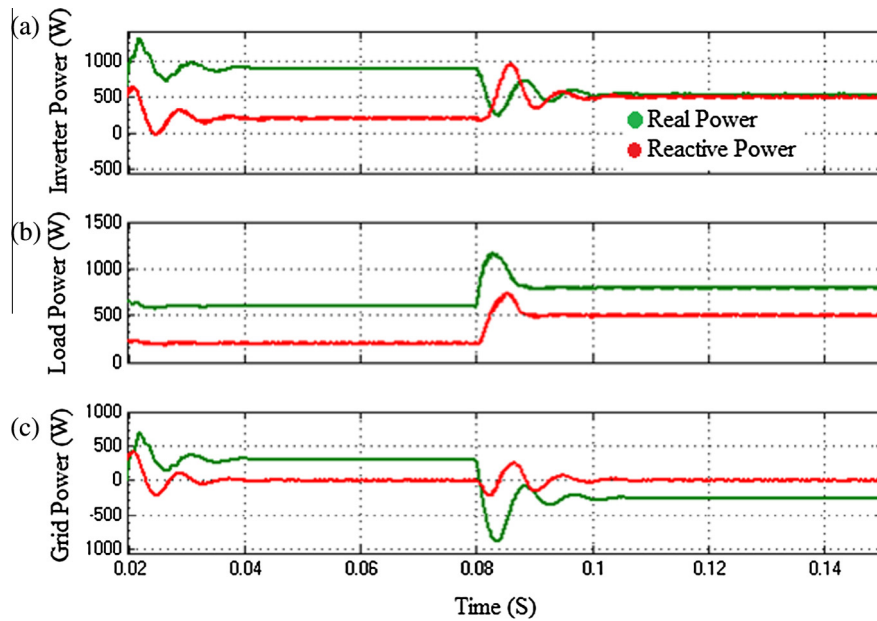


**Figure 14** Real and reactive power exchange under load variation – FOPI application. (a) Inverter, (b) load and (c) grid.

The grid current THD of the system is tabulated while employing PI and FO-PI controller for variable irradiation. It is noted from Table 4 that the THD content in the grid system using different frequency controllers lie below 5% of the IEEE standard and high frequency harmonics are eliminated effectively. The grid current THD of the system is obtained with PI controller during  $1000 \text{ W/m}^2$  and  $200 \text{ W/m}^2$  irradiation are 1.82% and 2.54% respectively. However, the application of FO-PI controller measures the THD content in the grid as 1.24% and 1.87%. The major reduction in the grid current THD of 31.87% is observed for the irradiation of  $1000 \text{ W/m}^2$ . Similarly, 26.37% reduction in THD is achieved during  $200 \text{ W/m}^2$  irradiation. The FFT analysis of the controllers is shown in Figs. 12 and 13.

**Table 5** Grid current THD during change in load.

Load		% THD	
$P$ (W)	$Q$ (VAR)	PI	FO-PI
600	200	1.82%	1.24%
700	600	3.32%	2.62%

### 3.2. Controller performance during change in load

The power factor control in the grid and the power distribution of the system is analyzed under change in load. Fig. 14 shows the power generation and distribution when load

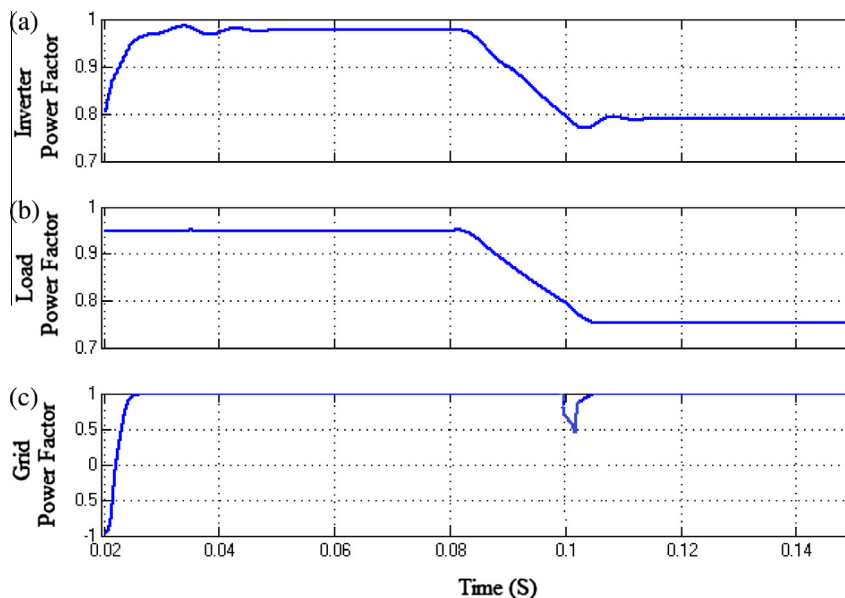


**Figure 15** Power factor variation during load variation – FOPI application. (a) Inverter, (b) load and (c) grid.

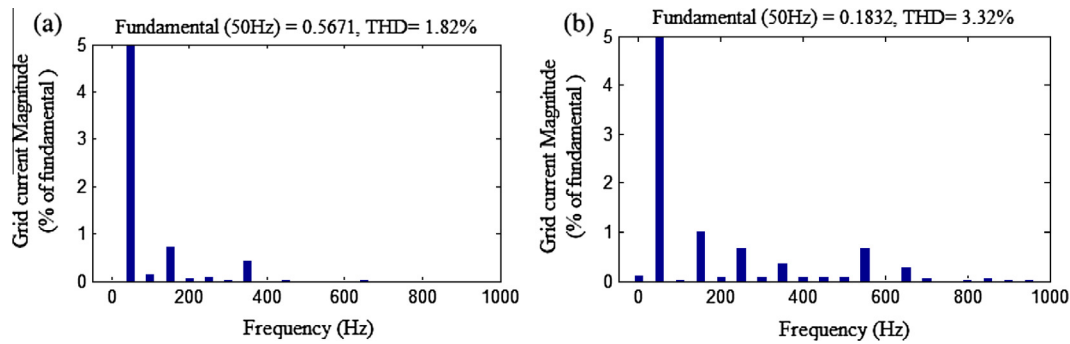


**Figure 16** FFT analysis of grid current THD during load variation – PI application. (a)  $P = 600$  W,  $Q = 200$  VAR and (b)  $P = 700$  W,  $Q = 600$  VAR.

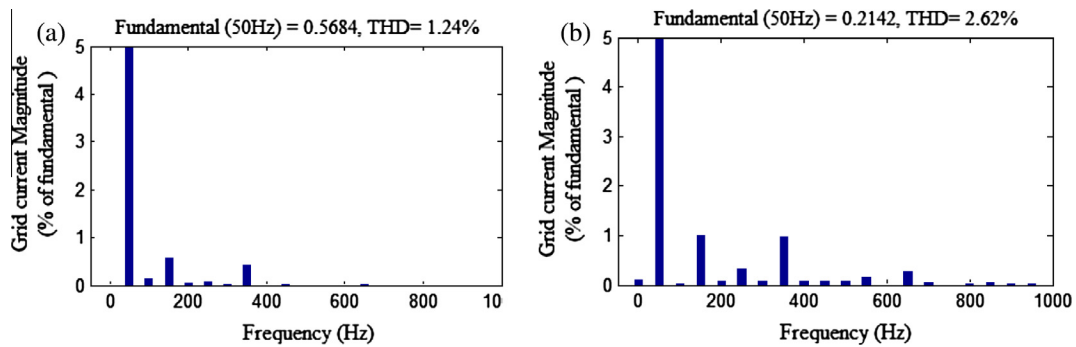


**Figure 17** FFT analysis of grid current THD during load variation – FO-PI application. (a)  $P = 600$  W,  $Q = 200$  VAR and (b)  $P = 700$  W,  $Q = 600$  VAR.

changes from 600 W, 200 VAR to 700 W, 600 VAR at  $t = 0.08$ . The real and reactive power requirement of the load is satisfied by the inverter power until  $t = 0.08$  s. Subsequently, the increased load of 700 W, 600 VAR is satisfied by supplying real power from the grid and the reactive power from the inverter. Therefore, the power factor varies during the load transition. Fig. 15 shows that the grid maintains unity power factor when the load power factor changes. The real and reactive power control during load variation is attained by regulating the direct and quadrature current components.

In addition, the application of PI and FO-PI controller in the grid-connected system is analyzed under change in load. The grid current THD of the system for load variation is given in Table 5. From Fig. 16, the grid current THD of the system is achieved with PI controller during the load changes 1.82% and 3.32% respectively. With the use of FO-PI, the reduction in the grid current THD of 31.87% is achieved when introducing load with high power factor. Similarly, 21% of reduction in the THD is obtained with low power factor loads. The FFT analysis of grid current during load variation is shown in Fig. 17 with FO-PI controller. The significant improvement in THD reduction is attained by FO-PI compared with the PI controller.

#### 4. Conclusion

In this paper, a decoupled control of grid connected PV system using FO-PI controller is presented. The Matlab/Simulink software is used to develop and simulate the system. The application of decoupled control strategy with FO-PI controller in

the grid connected system gives better results compared to PI controller in terms of system response, DC link regulation and output current control at the inverter end. The reduction in grid current THD and power factor control in the grid is obtained during any irradiation as well as load variation. The significant reduction in the grid current THD is achieved by injecting less oscillation current to the grid. This feature of FO-PI controller improves the system efficiency by reducing the losses caused by THD during the variable irradiation and load condition.

#### References

- [1] Kadri R, Gaubert JP, Champenois Gerard. An improved maximum power point tracking for photovoltaic grid-connected inverter based on voltage-oriented control. *IEEE Trans Ind Electron* 2011;58(1):66–74.
- [2] Rey-Boue AB, Garcia-Valverde R, Ruz-Vila F, Torrello-Ponce JM. An integrative approach to the design methodology for 3-phase power conditioners in photovoltaic grid-connected systems. *Energy Convers Manage* 2012;56:80–95.
- [3] Franco Luis Claudio, Pfitscher Luciano Lopes, Gules Roger. A new high static gain non-isolated DC–DC converter. In: 34th Annual IEEE power electronics specialist conference (PESC), 3. p. 1367–72.
- [4] Li Wuhua, Zhao Yi, Deng Yan, He Xiangning. Interleaved converter with voltage multiplier cell for high step-up and high efficiency conversion. *IEEE Trans Power Electron* 2010;25(9):2397–408.
- [5] Chen Shih-Ming, Liang Tsong-Juu, Yang Lung-Sheng, Chen Jiann-Fuh. A cascaded high step-up DC–DC converter with single

- switch for microsource applications. *IEEE Trans Power Electron* 2011;26(4):1146–53.
- [6] Samosir Ahmad Saudi, Taufiq, Shafie Abd Jaafar, Yatim Abdul Halim Mohd. Simulation and implementation of interleaved boost DC–DC converter for fuel cell application. *Int J Power Electron Drive Syst* 2011;1(2):168–74.
- [7] Hsieh Yi-Ping, Chen Jiann-Fuh, Liang Tsorng-Juu, Yang Lung-Sheng. Novel high step-up DC–DC converter with coupled-inductor and switched-capacitor techniques. *IEEE Trans Ind Electron* 2012;59(2):998–1007.
- [8] Chen Shih-Ming, Liang Tsorng-Juu, Yang Lung-Sheng, Chen Jiann-Fuh. A safety enhanced, high step-up DC–DC converter for AC photovoltaic module application. *IEEE Trans Power Electron* 2012;27(4):1809–17.
- [9] Changchien SK, Liang TJ, Chen JF, Yang LS. Step-up DC–DC converter by coupled inductor and voltage-lift technique. *IET Power Electron* 2010;3(3):369–78.
- [10] Soomro Amir Mahmood, Lingyu Xu, Khahro Shah Nawaz Farhan, Xiaozhong Liao. High output voltage based multiphase step-up DC–DC converter topology with voltage doubler rectifiers. *TELKOMNIKA Indones J Electr Eng* 2013;11(2):1063–8.
- [11] Prudente Marcos, Pfitscher Luciano L, Emmendoerfer Gustavo, Romaneli Eduardo F, Gules Roger. Voltage multiplier cells applied to non isolated DC–DC converters. *IEEE Trans Power Electron* 2008;23(12):871–87.
- [12] Yang Lung-Sheng, Liang Tsorng-Juu, Lee Hau-Cheng, Chen Jiann-Fuh. Novel high step-up DC–DC converter with coupled-inductor and voltage doubler circuits. *IEEE Trans Ind Electron* 2011;59(9):4196–206.
- [13] Rakesh Sharma, Vivek Agarwal. A high gain DC–DC converter with voltage multiplier. 5th Annual IEEE energy conversion congress and exposition (ECCE), 2013.
- [14] Su YX, Sun Dong, Duan BY. Design of an enhanced nonlinear PID controller. *Mechatronics* 2005;15(8):1005–24.
- [15] Maiti Deepyaman, Acharya Ayan, Chakraborty Mithun, Konar Amit, Janarthanan Ramadoss. Tuning PID and FOPID controllers using the integral time absolute error criterion. In: 4th IEEE international conference on information and automation for sustainability.
- [16] Podlubny Igor. Fractional-order systems and FOPID controllers. *IEEE Trans Autom Control* 1999;44(1):208–13.
- [17] Tsengenes G, Adamidis G. Investigation of the behavior of a three phase grid connected photovoltaic system to control active and reactive power. *Electr Power Syst Res* 2011;81(1):177–84.
- [18] Saccomando G, Svensson J. Transient operation of grid connected voltage source converter under unbalanced voltage conditions. In: Proc. IAS, Chicago, IL, 4. p. 2419–24.
- [19] Pandey A, Dasgupta N, Mukerjee AK. Design issues in implementing MPPT for improved tracking and dynamic performance. In: 32nd IEEE Annual Conference on Industrial Electronics (IECON'06). p. 4387–91.
- [20] Ruz F, Rey-Boué AB, Torrelo JM, Nieto A, Canovas FJ. Real time test benchmark design for photovoltaic grid-connected control systems. *Electr Power Syst Res* 2011;81:907–14.
- [21] Shen Miaosen, Peng Fang Zheng, Tolbert Leon M. Multilevel DC–DC power conversion system with multiple DC source. *IEEE Trans Power Electron* 2008;23(1):420–6.
- [22] Mohan Ned, Undeland Tore M, Robbins William P. Power electronics: converters, applications, and design. John Wiley & Sons Press; 2002.
- [23] D'Souza NS, Lopes LAC, Liu X. Comparative study of variable size perturbation and observation maximum power point trackers for PV systems. *Electr Power Syst Res* 2010;80:296–305.
- [24] Hassaine L, Olias E, Quintero J, Haddadi M. Digital power factor control and reactive power regulation for grid-connected photovoltaic inverter. *Renew Energy* 2009;34:315–21.
- [25] Albuquerque FL, Moraes AJ, Guimaraes GC, Sanhueza SMR, Vaz AR. Photovoltaic solar system connected to the electric power grid operating as active power generator and reactive power compensator. *Sol Energy* 2010;84:1310–7.
- [26] IEEE standard for interconnecting distributed resources with electric power systems. *IEEE Standard 1547*; 2003. p. 1–28.
- [27] Meyer R, Mertens A. Design and optimization of LCL filters for grid-connected converters. In: 15th International power electronics and motion control conference (EPE/PEMC), LS7a.1-1–LS7a.1-6.



**M. Lakshmi** received B.E. degree in Electrical and Electronics Engineering from Bharathidasan University, Tiruchirappalli, India, in 2003, M.E in Power Systems from Anna University, Chennai, India, in 2011 and pursuing Ph.D. degree in Electrical Engineering from VIT University, Chennai, India. Her current research interests include Application of Power Electronics in Power Systems, High-Power dc/dc converters and Renewable Energy Applications.



**Dr. S. Hemamalini** received B.E in Electrical and Electronics Engineering from Thiagarajar College of Engineering, Madurai, India, M. Tech in Power Systems and Ph.D from National Institute of Technology, Tiruchirappalli, India. She has teaching and research experience of about 20 years. Currently she is Professor in the School of Electrical Engineering, VIT University, Chennai, India. Her field of research interests are Power System Optimization, Power Electronics Applications in Power Systems, Reliability and Protection in Micro-grids, Electric Vehicles. She is a member of IEEE and also member in power and energy society, IEEE power electronics society and a lifetime member of ISTE.